particles

IMPACT FACTOR 1.7

CITESCORE 3.2

Article

A Multiple Scattering-Based Technique for Isotopic Identification in Cosmic Rays

Francesco Dimiccoli and Francesco Maria Follega

Special Issue

Innovative Techniques for Particle Physics in Space

Edited by

Dr. Francesco Maria Follega and Dr. Francesco Nozzoli

MDPI

https://doi.org/10.3390/particles7020027

particles

MDPI

Article

A Multiple Scattering-Based Technique for Isotopic Identification in Cosmic Rays

Francesco Dimiccoli [1,2,*,†] and Francesco Maria Follega [1,2,*,†]

[1] Department of Physics, University of Trento, Via Sommarive 14, 38122 Trento, Italy
[2] Trento Institute for Fundamental Physics and Applications (INFN-TIFPA), Via Sommarive 14, 38122 Trento, Italy
* Correspondence: francesco.dimiccoli@unitn.it (F.D.); francesco.follega@unitn.it (F.M.F.)
† These authors contributed equally to this work.

Abstract: Analyzing the isotopic composition of cosmic rays (CRs) provides valuable insights into the galactic environment and helps refine existing propagation models. A particular interest is devoted to secondary-to-primary ratios of light isotopic components of CRs, the measurement of which can provide complementary information with respect to secondary-to-primary ratios like B/C. Given the complexity of the concurrent measurement of velocity and momentum required to differentiate isotopes of the same Z, a task typically accomplished using magnetic spectrometers, existing measurements of these ratios only effectively characterize the low-energy region (below 1 GeV/nucl). This study introduces a novel technique for isotopic distinction in CRs at high energies up to 100 GeV/nucl based on multiple scattering, which, combined with the proposed measurement of velocity, represent an interesting alternative to magnetic spectrometers. The performance of this technique was assessed through a dedicated simulation using the GEANT4 package, with specific emphasis on Z = 1 isotopes.

Keywords: particle physics; detector; multiple scattering; RICH; isotope; spectrometer; space; simulation

Citation: Dimiccoli, F.; Follega, F.M. A Multiple Scattering-Based Technique for Isotopic Identification in Cosmic Rays. *Particles* **2024**, *7*, 477–488. https://doi.org/10.3390/particles7020027

Academic Editor: Hideaki Ohgaki

Received: 1 April 2024
Revised: 24 April 2024
Accepted: 29 April 2024
Published: 2 May 2024

1. Introduction

Cosmic rays species are categorized into primary and secondary species. The former come directly from acceleration sites, mainly Supernova Remnants (SNRs) via diffusive shock acceleration and the relativistic jets from Active Galactic Nuclei (AGN) [1,2]; the latter result from spallation reactions with the Interstellar Space Medium (ISM). Secondary nuclei like Li, Be, and B are more abundant in CRs than in the Solar System's average composition [3–6].

Interactions with the ISM not only alter the chemical composition of CRs, but also their isotopic composition. Studying specific CR isotopic ratios offers crucial insights into the galactic environment, complementing commonly used tools like the B/C ratio [7]. The interest is particularly high in the measurement of light secondary isotopic components (up to Z = 4). Thanks to their low mass and smaller interaction cross section with the ISM, they can probe a larger galactic volume compared to heavier secondaries like B [8].

Furthermore, specific isotopic ratios can provide unique information, due to the peculiar characteristics of each nucleus. An example is given by radioactive isotopes like ^{10}Be. The beryllium isotopic composition in CRs includes ^{10}Be, a radioactive isotope with a decay time of the same order of the expected residence time of CRs in the galaxy. Since ^{10}Be decays to ^{10}B before reaching the boundary of the galaxy, the ratio of unstable-to-stable secondary ^{10}Be/^{9}Be measures the galactic halo size L and, in general, the galactic propagation volume [9,10]. Another example is the case of ^{7}Li, which is expected to be a completely secondary nucleus like its lighter isotope ^{6}Li, while some studies show that lithium flux is higher than model predictions, hinting at the existence of primary lithium [11].

Lastly, is the peculiar case of deuterons (D), the most abundant secondary nucleus in CRs, believed to share the same origin in CRs as its isobar nucleus ^{3}He, namely being mainly formed from the fragmentation of primary ^{4}He nuclei. Nevertheless, experimental hints to a relevant excess of D, with respect to the expectations from secondary production alone, have been provided in the past, albeit with large errors, from the D/He measurements of CAPRICE [12] and SOKOL [13] experiments. These recent insights raised the interest about the nature of D nuclei, suggesting a primary nature of this specific isotope. Nevertheless, currently, there are no dedicated experiments operating for the detection of light isotopes.

Indeed, traditional experiments face challenges in directly measuring light isotope abundance in CRs due to the difficult isotopic separation from the main component and unfavorable signal/noise ratio. One of the most challenging cases is the D case: balloon-borne experiments and space instruments typically rely on mass spectrometers, but their limited resolution is a challenge, given the small ratio of D nuclei to p (~0.02).

Mass measurement, derived from momentum and velocity using the relativistic formula, is indirect:

$$m = \frac{|p|}{\beta}\sqrt{1-\beta^2} \quad (1)$$

where p is the particle momentum and β is the ratio of the particle velocity with the speed of light. Limited β resolution, often obtained through Time Of Flight (TOF) systems, constrains the energy range for isotopic distinction due to rapid relativistic saturation of β to 1. An exception was the CAPRICE experiment [12], using a Cherenkov detector for D/He measurement in the 18–22 GeV/nucleon range. Using a calorimetric approach, SOKOL instead claimed a measurement of D/He in the TeV energy range, suggesting a surprisingly high D abundance. A high-precision measurement at an energy higher than a few GeV/nucleon is still missing [14] and could shed light on the origin hypotheses for D.

For the same reasons, high-energy measurements of light isotopic ratios are extremely rare, since few experiments offer the possibility of a joint measurement of momentum and velocity with the precision requirements needed for isotopic distinction. A notable example is the AMS-02 detector, which is expected to extend up to 10 GeV/nucleon the range of percent level measurement precision in CR light isotopic abundance [7,15].

2. Measurement of the Energy per Nucleon with a RICH Detector

Isotopes of equal charge and velocity can be discriminated on the basis of their momentum, as shown in Equation (1). Particle kinetic energy per nucleon E_k/A can be obtained from a measurement of particle velocity (β = v/c), through the relation

$$E_k/A = m_n(\gamma - 1) \quad (2)$$

where m_n is the mass of the average nucleon (m_n = 0.938 GeV/c^2). A precise velocity measurement in the 10–100 GeV/nucleon energy range can be obtained using a Cherenkov detector.

A Ring Imaging Cherenkov (RICH) detector design was devised for this purpose, based on a 1 cm thick layer of silica aerogel radiator with a typical spectral index of n = 1.05 and density of 0.2 g/cm^3 [16–18].

The crossing of a charged particle with a kinetic energy in the 10–100 GeV/nucleon range in such radiator produces Cherenkov cones with aperture given by $\arccos(1/n\beta)$ in the range 0.836–0.841 rad. A 0.5 cm thick Pyrex glass spherical mirror with curvature radius R_m = 1 m and diameter = 0.5 m was placed at a distance d = 0.5 m behind the radiator in the particle propagation direction. It refocused the Cherenkov photons in a ring on a planar detecting surface adjacent to the radiator plane, as shown in Figure 1. Spherical mirror design like the one proposed here are in use in several high-energy physics experiments [19,20], since the refocusing of the photons allows to exploit relatively large radiators, while keeping the overall detector structure rather compact. A suitable choice for the photon detecting surface is an array of 30 × 30 μm Silicon Photomultipliers (SiPMs) [21]. It guarantees both the necessary spatial resolution and detection efficiency while maintaining a low material

budget. The RICH design performance was simulated using GEANT4 to estimate the resolution of a possible velocity measurement for the isotopic discrimination of D above 10 GeV/nucleon. Effects such as the Cherenkov photons propagation, Rayleigh scattering, and photon auto-absorbing were included in the simulation, modeling the optical properties of Silica aerogel [22]. Given the purpose of this feasibility study, only perpendicular tracks were simulated. Efficiency and resolution losses given by the inclination of the tracks in a realistic isotropic flux go beyond the purposes of this work. The performance, measured on four monochromatic beams of D at E_k/A of 15, 32, 52, and 80 GeV/nucleon, was consistent with those of similar designs in used in other experiments [23], ranging from 0.2% to ~8% in the target energy range (Figure 2).

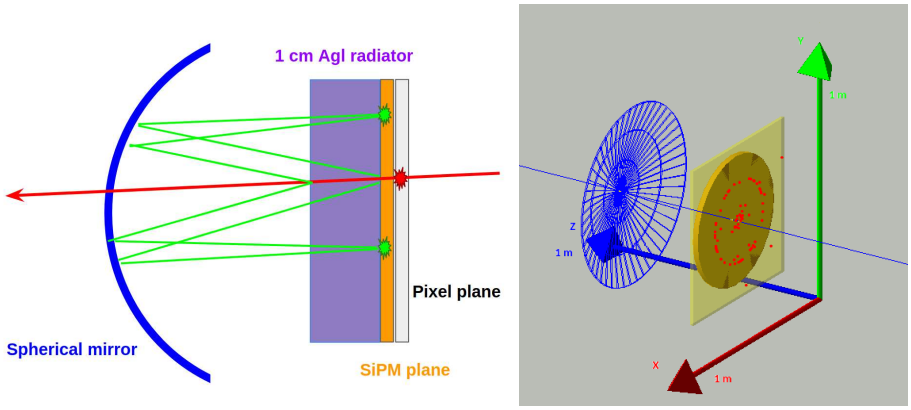

Figure 1. On the left, a graphical scheme of the RICH design devised for this work is shown. The dimensions of the components are not to scale for display purposes. On the right, visualization of the RICH geometry implemented in the GEANT4 simulation, with a simulated D event of generated energy of 50 GeV/nucleon. In the visualization, the hits from Cherenkov photons produced in the aerogel radiator (yellow circle) by the incoming particles are visible in red on the SiPM plane (yellow semitransparent square). The three colored arrows indicate the reference frame used for the visualization, with the labels representing the dimension scale.

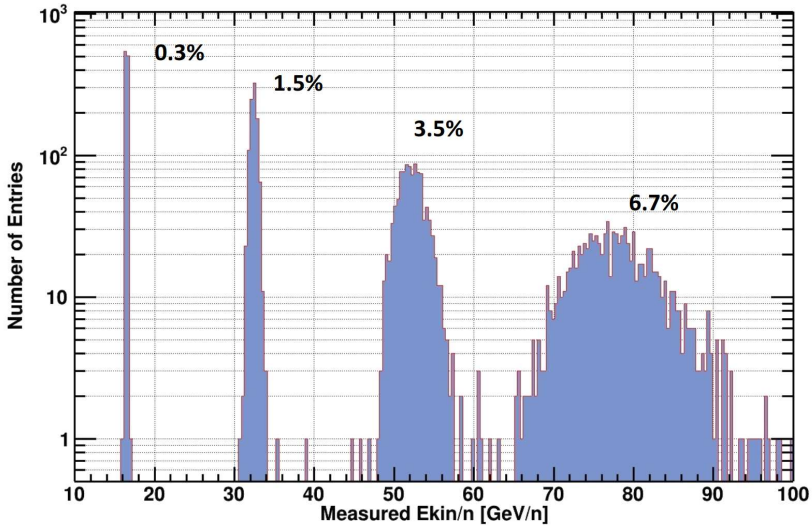

Figure 2. Performance of the proposed RICH design: reconstructed E_k/n for four monochromatic D beams of 16, 32, 52, and 80 GeV/nucleon. Measured resolution σ_{E_k}/E_k is also quoted close to each distribution.

3. Using Multiple Scattering for Isotopic Distinction in CRs

To explore the energy range above 10 GeV/nucleon, the precision in momentum measurement is also a challenge, as it is proportional to the mass. Since, at large particle

momenta, the resolution of magnetic spectrometers degrades proportionally to momentum itself [24], a high tracking accuracy and/or bending power of the magnet is required, increasing the cost and the complexity of the experiment. Solutions like these ones are usually reached using superconducting magnets [4], which are only recently being prototyped for future space missions [25–28].

This reason motivates the exploration of a new technique for isotopic distinction in CRs that does not rely on a direct measurement of momentum (i.e., does not need a magnetic spectrometer), but is based on a measurement of the multiple scattering of cosmic-charged particles in high-density targets. The proposed isotopic distinction method exploits the different scattering angles that particles of the same velocity experience, having different masses. The average deviation from the original trajectory that a charged particle experiences when it crosses a target is described by the multiple scattering(MS) formula [29] (in natural units):

$$\Theta_{MS} = \frac{13.6\,\mathrm{MeV}}{\beta p} z\sqrt{x/X_0}\left[1 + 0.038\ln(x/X_0)\right] \quad (3)$$

where $p = m\beta\gamma$ is the particle momentum of a particle of a given mass m, z is the particle charge, and x/X_0 is the value of the thickness of material traversed by the particle in units of radiation length.

We can apply this concept to Z = 1 isotopes, namely protons and deuterons. A particle with approximately double the mass of a proton, such as a D, traverses a target and the average deviation it experiences is reduced by approximately half compared to that of protons.

Several MS measurement stations along the charged particle track can, together, provide a measurement of Θ_{MS}. Assuming that the displacement measurement performed by every station is independent from the others, the precision in the Θ_{MS} measurement is only limited by the total number of measuring stations along the track.

A proposed detector able to perform this measurement, a Multiple Scattering Isotope Separator (MSIS), was devised and tested in a dedicated GEANT4 simulation. Its design and expected performance are described in the next section.

A Proposal for a Multiple Scattering-Based Isotope Separator

Previous studies have shown the possibility of reconstructing particle momentum on the base of the detected multiple scattering angle [30]. In this paragraph, we present a proposal for a Multiple Scattering Isotope Separator (MSIS) based on a simple geometry. The elementary constituent of the MSIS is a PPT module (Plane–Plane–Target). It comprises two silicon plane surfaces, each measuring 33 × 33 cm^2 and 7 mm thick, with a 3 cm separation between them, followed by, along the particle propagation direction, a 6 mm thick Pb target adjacent to the second plane, as shown in Figure 3. The two silicon planes have the purpose of measuring the direction of the incoming particle, while the high-density and high-Z Pb target has the purpose of deviating the trajectory according to Equation (3). Details on the required performance of the silicon tracking planes for this design are provided in Section 4.

The subsequent PPT module measures the deviated trajectory by determining both the new trajectory and its displacement d with respect to the linear interpolation of the preceding one. To ensure that displacements are sufficiently large compared to the spatial resolution σ_d offered by the silicon plane, the next station has to be positioned at a distance $S \geq N \cdot \sigma_d / \tan(\Theta_{MS})$ from the previous one, along the direction of the track, where N is the desired significance of the measurement. For this design, a spacing S = 12 cm was selected, which, combined with the chosen thickness of the Pb targets, represented a suitable compromise between the separation power of Z = 1 isotopes and the overall dimensions and total grammage of the MSIS. These parameters can be tuned to optimize performance for isotopes of higher Z.

The measurement of the displacement was repeated iteratively, with every PPT module measuring the displacement of the trajectory with respect to the one measured by the previous one and deviating the trajectory again before the measurement by the following one.

A realistic design of the MSIS includes a series of eight consequent PPT modules, and a final silicon plane to measure the impact position, allowing a total of eight independent measurements of displacement. The average displacement can then be obtained as an average of all the measurements, acting as a discriminant for isotopes selected in the same interval of E_k/A (i.e., velocity).

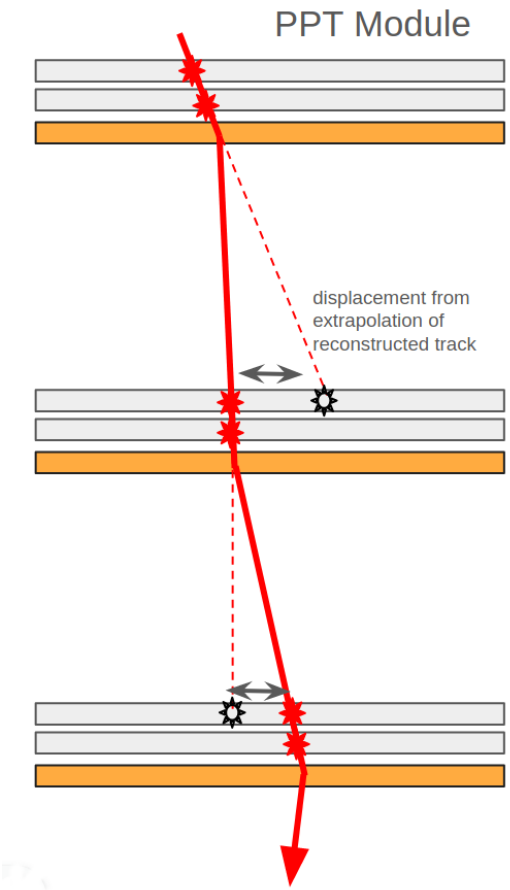

Figure 3. In this figure, a schematic of the working principle of the MSIS is shown. Three subsequent PPT modules are depicted. In red, the scattered track is shown with the hits on each silicon module (gray). The lead layers are drawn in orange. The three depicted modules allow for two independent displacement measurements. In a realistic detector, more modules would be present. To exploit the scattering induced by the last lead target, an extra silicon layer is needed.

The eight Pb targets account for a total of 0.3 nuclear interaction lengths and 8.6 X_0. Inelastic and hadronic interactions inside the MS detector are expected to be non-negligible, introducing, not only efficiency problems due to loss of events, but also creating spurious hits in the silicon planes. Such problems are addressed in Section 4, where the performance of the MSIS detector is also discussed.

4. Simulation of the MSIS Design

According to Equation (3), a D in the 10–100 GeV/nucleon E_k/A energy range crossing a 6 mm thick Pb target experiences an average MS induced angular deviation of ≈0.05–0.5 mrad. A spacing S = 12 cm between subsequent PPT modules would result, for a D, in an average displacement from ≈10 μm to ≈100 μm in the energy range of interest. A suitable choice for this measurement is represented by ALPIDE pixel sensors (28 × 28 μm^2), which, thanks to

cluster size interpolation, can reach a sub-pixel spatial resolution of the order of $\sigma_d = 5$ µm [31], with low material budget $\approx 0.005\ X_0$ per tracking plane. Tracking detectors of this kind have already been produced and integrated in space detectors [32,33]. Moreover, their use is planned in future missions [25].

The ensemble of the eight PPT modules, spanning a total length of 108 cm, were simulated considering such pixelation of the tracking silicon planes, using the GEANT4 package [34]. The performance of the apparatus was evaluated using simulated beams of p and D generated in different intervals of E_k/A spanning the 10–100 GeV/nucleon energy range. The same considerations stated in Section 2 about the inclination of the simulated tracks were also considered valid in this analysis.

To also include in the performance evaluation the effect of a realistic precision in the E_k/A measurement, the width of the generated E_k/A intervals was chosen according to the measured E_k/A resolution obtained from the RICH apparatus described in Section 2.

The simulation made use of the standard QGSP-BIC physics list [34], which includes all the principal electromagnetic and hadronic processes, as well as radioactive decay and neutron transport processes. Figure 4 shows the simulated geometry, with the interaction of a simulated CR event.

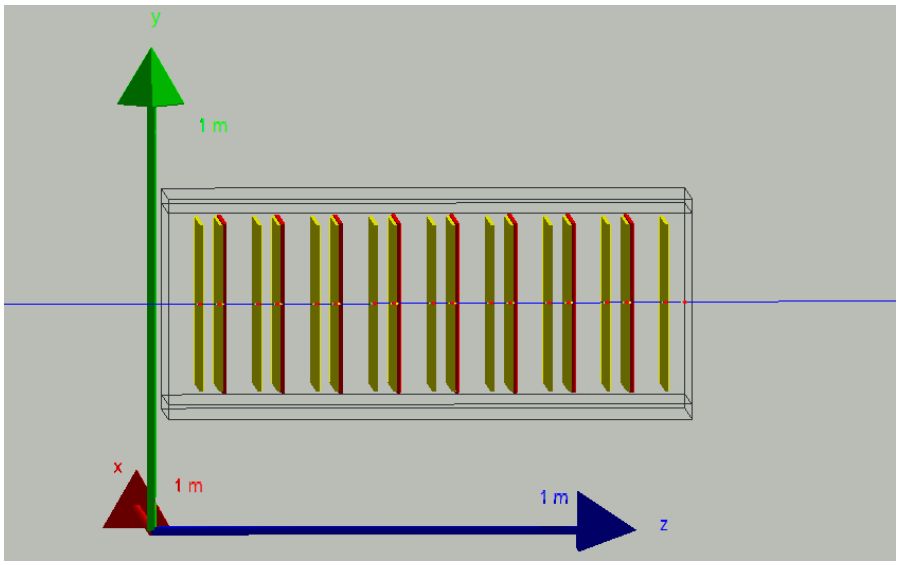

Figure 4. Graphical view of the GEANT4 simulation of the MSIS, with a simulated D event of generated energy 50 GeV/nucleon. Yellow volumes represent the tracking planes, while red volumes represent Pb targets. The blue track represents the trajectory of the particle and the red circles are hits on the detector materials. The three colored arrows indicate the reference frame used for the visualization, with the labels representing the dimension scale.

The coordinates of each interaction point between the incident particle and its secondary particles with every silicon plane were recorded, considering the discretization in the measurements and accounting for dead zones resulting from the pixelation of the plane.

4.1. Effect of Interactions

Multiple high-density targets along the particle trajectory increase the probability of interactions with generation of secondaries that can confuse the main track reconstruction. Furthermore, hadronic interactions in the target can cause the loss of primary particles. This latter efficiency loss was evaluated from the simulation to range from 10% to 15% in the 10–100 GeV/nucleon E_k/A range. Delta ray electrons are the main source of spurious hits in tracking planes. However, simulation results (see Figure 5) demonstrate that these hits are well separated from the main track. Indeed, these particles are lighter and are generated with a lower kinetic energy with respect to the primary particle; this fact increases the multiple scattering angle, making it easier to distinguish them from primary tracks.

Cumulative displacement analysis of particle hits in the first tracking plane of each PPT module reveals that secondary hits are overwhelmingly concentrated at displacements greater than 1 mm. From a cut and count analysis on the distributions of Figure 5, the results show that searching for primary hits within a 1 mm radius yields a mis-classification rate of below 0.05%.

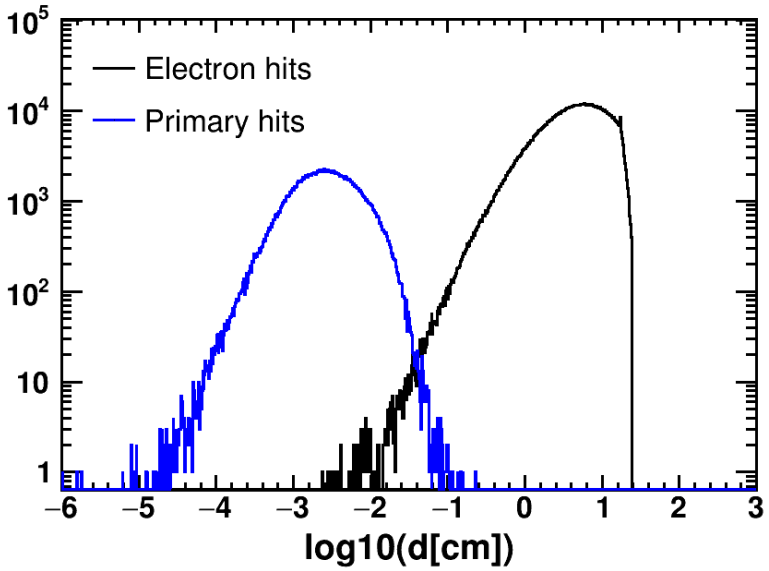

Figure 5. The blue line shows the distribution of calculated displacement between the interaction point of the primary particle on a given tracking layer and the extrapolated position of the primary trajectory, reconstructed with the previous PPT module. The black line shows the distribution of calculated displacement between the interaction points of the secondary electrons on the same tracking layer and the extrapolation of the primary trajectory measured in the previous PPT module.

4.2. Reconstruction and Performance

To apply the technique described in Section 3 and calculate the MS average displacement, the algorithm described as follows was used:

1. Starting from the position of two hits measured in the tracking planes of the first PPT module, a linear trajectory is calculated.
2. The trajectory is extrapolated to the position of the first tracking plane of the next PPT module.
3. The distance between the extrapolation position and the closest measured hit in the first plane of the second PPT module is taken as displacement measurement (if no hit is found within a 1 mm radius from the extrapolation position, the event is discarded).
4. The measurement of displacement induced by the second PPT module is then performed in the same way using the third one and so on, up to the end of the detector. In this way, eight single d_i measurements are obtained.
5. To further improve the precision of the average displacement measurement, displacements calculated using all the couples of subsequent PPT planes are added in the average process. Such measurements are multiplied by a factor of $1/\sqrt{2}$ to account for the double target thickness traversed, according to Equation (3). In this way, seven additional d_i^C displacement measurements are obtained, considering all the subsequent PPT pairs.

The average displacement $< d >$ is calculated as follows:

$$< d >= \frac{\sum_{i=0}^{N_{PPT}} d_i}{N_{PPT}} + \frac{\sum_{i=0}^{N_C} d_i^C/\sqrt{2}}{N_C} \quad (4)$$

where d_i is the displacement reconstructed on each silicon plane after the lead target, with $N_{PPT} = 8$ being the number of measurement stations, and d_i^C the displacement reconstructed from each silicon plane couple, with $N_C = 7$ being the total number of possible subsequent couples of measurement stations.

An example of the performance of this technique in separating D from p when they have the same kinetic energy per nucleon is shown in Figure 6, as a result of the simulation described above. The binning used in the histograms shown in the picture is representative of the real spatial resolution of the singular displacement measurements.

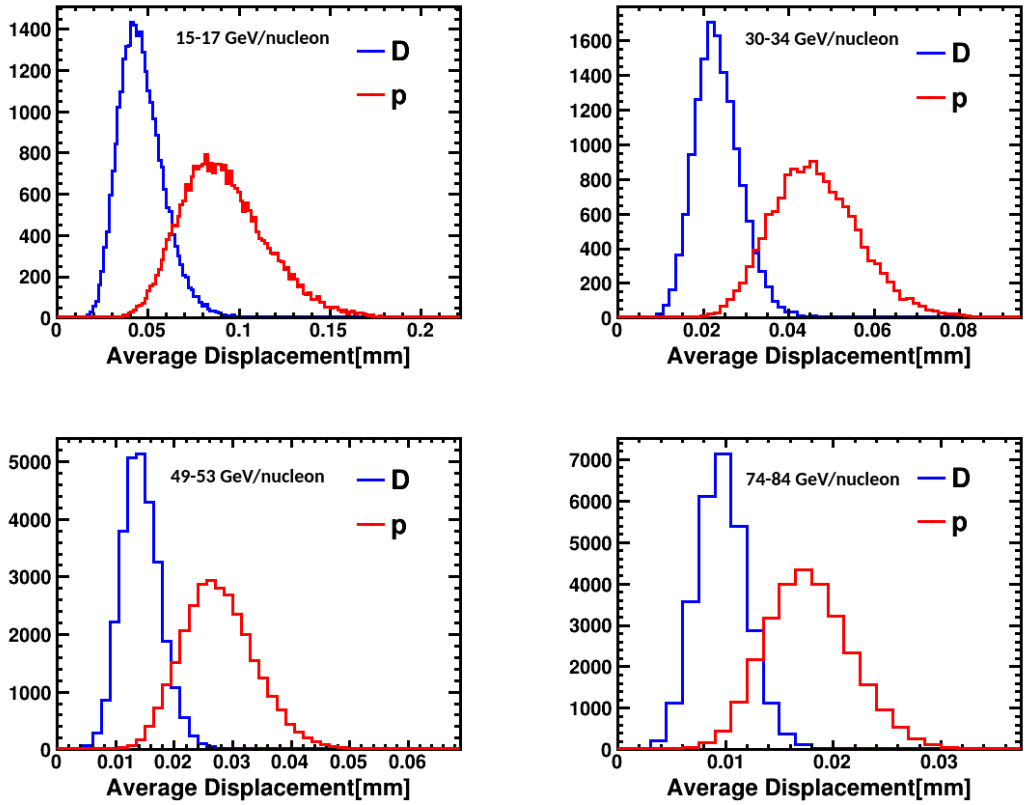

Figure 6. Distributions of average displacements measured in four simulated beams of D (blue) and p (red) in different E_k/A ranges by the MSIS. (**Top left**): 16–17 GeV/nucleon, (**top right**): 30–34 GeV/nucleon, (**bottom left**): 49–53 GeV/nucleon, (**bottom right**): 74–84 GeV/nucleon.

The upper plot in Figure 7 demonstrates the level of separation of the two populations. In a scenario where individual events are classified as D in the 10–100 GeV/nucl range through a simple cut-and-count method, the background efficiency (ϵ_B) would be below the 5% level, while maintaining a good D identification efficiency (ϵ_S) of at least 80% in a wide range of energies. The same figure also depicts the MSIS rejection capability for p when detecting D signals, quantified as the ratio of signal efficiency to background efficiency (ϵ_S/ϵ_B). This quantity is the inverse of the probability of misidentifying an incoming proton as a D event. Such probability results are below 3% for D efficiencies surpassing 60%.

Considering a D/p ratio of 2.5%, in line with current measurements in the energy range [12], the resulting signal-to-noise ratio allows for a template-fit-based analysis, such as one outlined in [35], granting a fit statistical error $\leq 1\%$ when a number of D events ≥ 1000 is gathered. This approach enables a precise separation of D and p distributions, facilitating a high-precision measurement of the D/p abundance ratio in CRs.

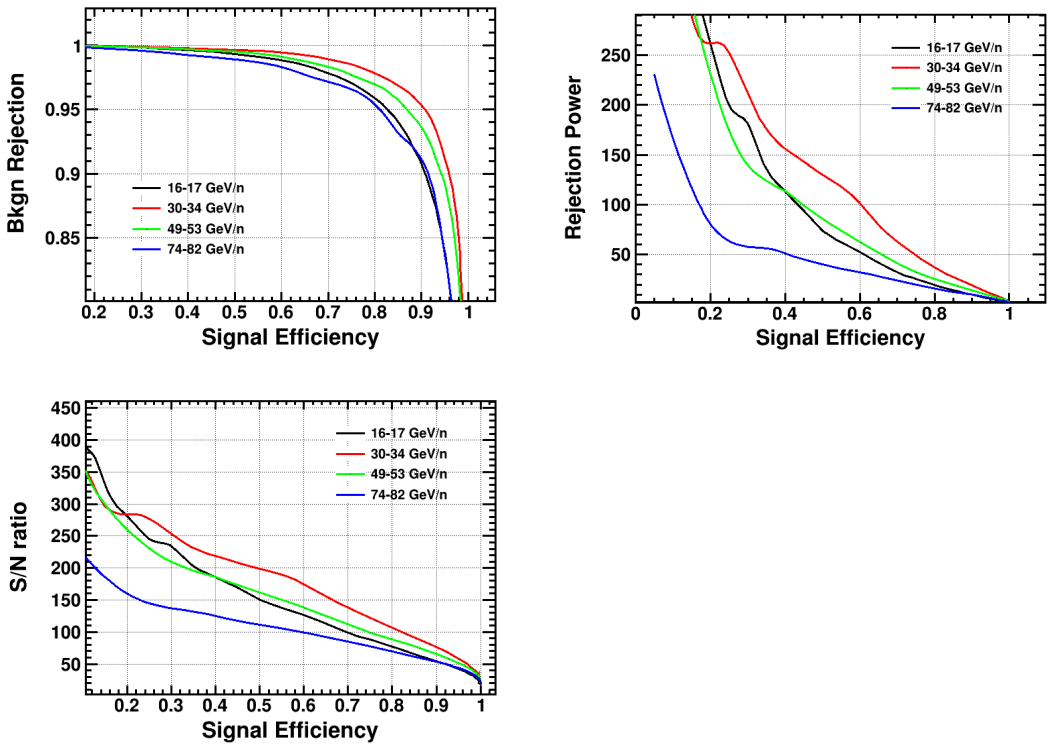

Figure 7. (**Top left**): performance of the MS displacement discrimination in terms of background rejection ($1 - \epsilon_B$) of p as a function of efficiency on D signal. (**Top right**): performance in terms of rejection power of p background (ϵ_S/ϵ_B) as a function of efficiency on D signal. (**Bottom**): expected signal/noise ratio ($D/\sqrt{p}$) for an injected D/p ratio of 0.025 as a function of efficiency on D, assuming to have statistical error on D $\leq$ 1% (D counts $\geq$ 10,000).

5. Concept of a Prototype for Isotope Measurements in Flight

The aforementioned design for a RICH and MSIS detector can be combined in a prototype. In Figure 8, a possible design is shown. In this case, a RICH detector is used in combination with an MSIS with eight subsequent PPT stations, plus a final couple of pixel planes.

This whole structure has a total net weight 60 Kg (not including mechanics or electronics) and a volume of approximately 60 cm $\times$ 60 cm $\times$ 150 cm, making this design approximately two orders of magnitude smaller in volume and mass than to current and future operating experiments like AMS-02 or GAPS [36]. This simple prototype would achieve an overall geometric acceptance on the order of 100 cm^2 sr. Its lightweight design makes it ideal for future balloon flight missions, where at least 30 days of data-taking are expected for each launch. During this period, the flux of D across the entire energy interval can be measured with a statistical error ranging from 0.1% to 3%.

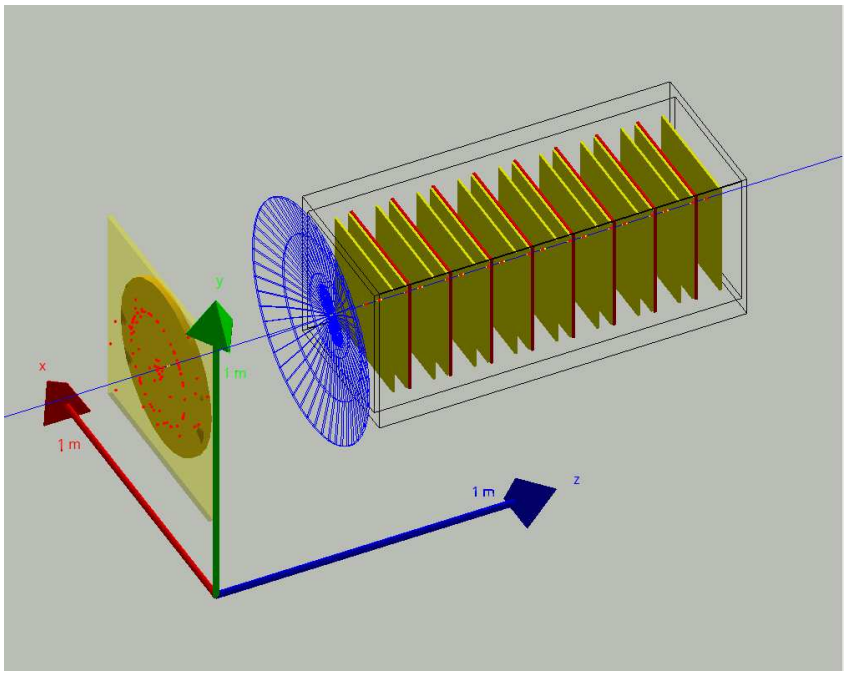

Figure 8. A GEANT4 simulation for a detector prototype. A deuterium nucleus is shot and traverses the entire the detector apparatus. In the figure, the blue line represents the trajectory of the primary particle, and the red dots are the energy deposits in the sensitive detectors. The three colored arrows indicate the reference frame used for the visualization, with the labels representing the dimension scale.

6. Conclusions

A new technique for isotopic distinction in CRs was presented, based on the evaluation of the different magnitudes of the average multiple scattering deviation induced by Pb targets on the trajectory of different isotopes with the same velocity.

The proposed technique relies on the multiple measurement of particle trajectory before and after the traversing of 0.6 cm thick targets of Pb. A preliminary detector design able to perform the measurement and its performance were discussed and evaluated on simulated hydrogen beams composed of p and D nuclei.

The technique was proven to be effective in discriminating vertical beams of D at different E_k/A in the range 10–100 GeV/nucl from p at the same kinetic energy per nucleon with a percent level background efficiency. Such a discrimination power allows to separate the two populations with a template fit approach.

A first hypothesis for a small prototype, designed for balloon flight, was described. This lightweight measurement device, combined with a proposed design of a Cherenkov detector, itself simulated, can be effectively exploited to obtain isotopic distinction for Z = 1 in CRs, in energy ranges still unexplored by current experiments.

Author Contributions: Conceptualization, F.M.F. and F.D.; methodology, F.M.F. and F.D.; software, F.M.F. and F.D.; validation, F.M.F. and F.D.; formal analysis, F.M.F. and F.D.; investigation, F.M.F. and F.D.; resources, F.M.F. and F.D.; data curation, F.M.F. and F.D.; writing—original draft preparation, F.M.F. and F.D.; writing—review and editing, F.M.F. and F.D.; visualization, F.M.F. and F.D.; supervision, F.M.F. and F.D.; project administration, F.M.F. and F.D.; All authors have read and agreed to the published version of the manuscript.

Funding: This research received no external funding

Data Availability Statement: No new data were created or analyzed in this study. Data sharing is not applicable to this article.

Conflicts of Interest: The authors declare no conflicts of interest.

References

1. Bell, A.R. The acceleration of cosmic rays in shock fronts—I. *Mon. Not. R. Astron. Soc.* **1978**, *182*, 147–156. [CrossRef]
2. Longair, M.S. *High Energy Astrophysics*, 3rd ed.; Cambridge University Press: Cambridge, UK, 2011.
3. Castellina, A.; Donato, F. Diffusion coefficient and acceleration spectrum from direct measurements of charged cosmic ray nuclei. *Astropart. Phys.* **2005**, *24*, 146–159. [CrossRef]
4. Ahlen, S.P.; Greene, N.R.; Loomba, D.; Mitchell, J.W.; Bower, C.R.; Heinz, R.M.; Mufson, S.L.; Musser, J.; Pitts, J.J.; Spiczak, G.M.; et al. Measurement of the Isotopic Composition of Cosmic-Ray Helium, Lithium, Beryllium, and Boron up to 1700 MeV per Atomic Mass Unit. *Astrophys. J.* **2000**, *534*, 757. [CrossRef]
5. Aguilar, M.; Ali Cavasonza, L.; Alpat, B.; Ambrosi, G.; Arruda, L.; Attig, N.; Aupetit, S.; Azzarello, P.; Bachlechner, A.; Barao, F.; et al. Observation of the Identical Rigidity Dependence of He, C, and O Cosmic Rays at High Rigidities by the Alpha Magnetic Spectrometer on the International Space Station. *Phys. Rev. Lett.* **2017**, *119*, 251101. [CrossRef]
6. Aguilar, M.; Ali Cavasonza, L.; Ambrosi, G.; Arruda, L.; Attig, N.; Aupetit, S.; Azzarello, P.; Bachlechner, A.; Barao, F.; Barrau, A.; et al. Observation of New Properties of Secondary Cosmic Rays Lithium, Beryllium, and Boron by the Alpha Magnetic Spectrometer on the International Space Station. *Phys. Rev. Lett.* **2018**, *120*, 021101. [CrossRef] [PubMed]
7. Aguilar, M.; Ali Cavasonza, L.; Ambrosi, G.; Arruda, L.; Attig, N.; Bachlechner, A.; Barao, F.; Barrau, A.; Barrin, L.; Bartoloni, A.; et al. Properties of Cosmic Helium Isotopes Measured by the Alpha Magnetic Spectrometer. *Phys. Rev. Lett.* **2019**, *123*, 181102. [CrossRef] [PubMed]
8. Coste, B.; Derome, L.; Maurin, D.; Putze, A. Constraining Galactic cosmic-ray parameters with $Z \leq 2$ nuclei. *A&A* **2012**, *539*, A88. [CrossRef]
9. Feng, J.; Tomassetti, N.; Oliva, A. Bayesian analysis of spatial-dependent cosmic-ray propagation: Astrophysical background of antiprotons and positrons. *Phys. Rev. D* **2016**, *94*, 123007. [CrossRef]
10. Weinrich, N.; Boudaud, M.; Derome, L.; Génolini, Y.; Lavalle, J.; Maurin, D.; Salati, P.; Serpico, P.; Weymann-Despres, G. Galactic halo size in the light of recent AMS-02 data. *A&A* **2020**, *639*, A74. [CrossRef]
11. Boschini, M.J.; Torre, S.D.; Gervasi, M.; Grandi, D.; Jóhannesson, G.; Vacca, G.L.; Masi, N.; Moskalenko, I.V.; Pensotti, S.; Porter, T.A.; et al. Inference of the Local Interstellar Spectra of Cosmic-Ray Nuclei $Z \leq 28$ with the GalProp–HelMod Framework. *Astrophys. J. Suppl. Ser.* **2020**, *250*, 27. [CrossRef]
12. Papini, P.; Piccardi, S.; Spillantini, P.; Vannuccini, E.; Ambriola, M.; Bellotti, R.; Cafagna, F.; Ciacio, F.; Circella, M.; Marzo, C.N.D.; et al. High-Energy Deuteron Measurement with the CAPRICE98 Experiment. *Astrophys. J.* **2004**, *615*, 259. [CrossRef]
13. Turundaevskiy, A.; Podorozhnyi, D. High energy deuterons in cosmic rays registered by the SOKOL satellite experiment. *Adv. Space Res.* **2017**, *59*, 496–501. [CrossRef]
14. Maurin, D.; Ahlers, M.; Dembinski, H.; Haungs, A.; Mangeard, P.S.; Melot, F.; Mertsch, P.; Wochele, D.; Wochele, J. A cosmic-ray database update: CRDB v4.1. *Eur. Phys. J. C* **2023**, *83*. [CrossRef]
15. Budrikis, Z. A decade of AMS-02. *Nat. Rev. Phys.* **2021**, *3*, 308. [CrossRef]
16. Wang, P.; Beck, A.; Korner, W.; Scheller, H.; Fricke, J. Density and refractive index of silica aerogels after low- and high-temperature supercritical drying and thermal treatment. *J. Phys. Appl. Phys.* **1994**, *27*, 414. [CrossRef]
17. PEREIRA, R. The RICH detector of the AMS-02 experiment: Status and physics prospects. In Proceedings of the Astroparticle, Particle and Space Physics, Detectors and Medical Physics Applications, Como, Italy, 8–12 October 2007; World Scientific: Singapore, 2008. [CrossRef]
18. Giovacchini, F. The RICH detector of the AMS-02 experiment aboard the International Space Station. *Nucl. Instrum. Methods Phys. Res. Sect. A Accel. Spectrom. Detect. Assoc. Equip.* **2023**, *1055*, 168434. [CrossRef]
19. Calabrese, R.; Fiorini, M.; Luppi, E.; Minzoni, L.; Slazyk, I.; Tomassetti, L.; Bartolini, M.; Cardinale, R.; Fontanelli, F.; Petrolini, A.; et al. Performance of the LHCb RICH detectors during LHC Run 2. *J. Instrum.* **2022**, *17*, P07013. [CrossRef]
20. Abbon, P.; Alekseev, M.; Angerer, H.; Apollonio, M.; Birsa, R.; Bordalo, P.; Bradamante, F.; Bressan, A.; Busso, L.; Chiosso, M.; et al. The COMPASS RICH-1 detector upgrade. *Eur. Phys. J. Spec. Top.* **2008**, *162*, 251–257. [CrossRef]
21. Ambrosi, G.; Ambrosio, M.; Aramo, C.; Bertucci, B.; Bissaldi, E.; Bitossi, M.; Boiano, A.; Bonavolontà, C.; Capasso, M.; Circiello, A.; et al. High-Density Near-Ultraviolet Silicon Photomultipliers: Characterization of photosensors for Cherenkov light detection. *Nucl. Instrum. Methods A* **2023**, *1049*, 168023. [CrossRef]
22. Altamura, A.; Mauro, A.D.; Nappi, E.; Nicassio, N.; Emmerik, M.v.; Volpe, G. Aerogel characterization for RICH applications. In Proceedings of the 2023 9th International Workshop on Advances in Sensors and Interfaces (IWASI), Monopoli, Italy, 8–9 June 2023; pp. 211–216. [CrossRef]
23. Albrecht, E.; Baum, G.; Birsa, R.; Bradamante, F.; Braem, A.; Bressan, A.; Chapiro, A.; Cicuttin, A.; Ciliberti, P.; Colavita, A.; et al. COMPASS RICH-1. *Nucl. Instrum. Methods A* **2003**, *502*, 112–116. [CrossRef]
24. Glusckstern, R.L. Uncertainties in track momentum and direction, due to multiple scattering and measurement errors. *Nucl. Instr. Methods* **1963**, *24*, 381. [CrossRef]
25. Battiston, R.; Bertucci, B.; Adriani, O.; Ambrosi, G.; Baudouy, B.; Blasi, P.; Boezio, M.; Campana, D.; Derome, L.; De Mitri, I.; et al. High precision particle astrophysics as a new window on the universe with an Antimatter Large Acceptance Detector In Orbit (ALADInO). *Exp. Astron.* **2021**, *51*, 1299–1330. [CrossRef]

26. Schael, S.; Atanasyan, A.; Berdugo, J.; Bretz, T.; Czupalla, M.; Dachwald, B.; Doetinchem, P.; Duranti, M.; Gast, H.; Karpinski, W.; et al. AMS-100: The Next Generation Magnetic Spectrometer in Space—An International Science Platform for Physics and Astrophysics at Lagrange Point 2. *Nucl. Instrum. Methods Phys. Res. Sect. A Accel. Spectrom. Detect. Assoc. Equip.* **2019**, *944*, 162561. [CrossRef] [PubMed]
27. Dam, M.; Burger, W.; Carpentiero, R.; Chesta, E.; Iuppa, R.; de Rijk, G.; Rossi, L. Design and Modeling of AMaSED-2: A High Temperature Superconducting Demonstrator Coil for the Space Spectrometer ARCOS. *IEEE Trans. Appl. Supercond.* **2022**, *32*, 4500105. [CrossRef]
28. Dam, M.; Burger, W.J.; Carpentiero, R.; Chesta, E.; Iuppa, R.; Kirby, G.; de Rijk, G.; Rossi, L. Manufacturing and testing of AMaSED-2: A no-insulation high-temperature superconducting demonstrator coil for the space spectrometer ARCOS. *Supercond. Sci. Technol.* **2022**, *36*, 014007. [CrossRef]
29. Zyla, P.A.; Barnett, R.M.; Beringer, J.; Dahl, O.; Dwyer, D.A.; Groom, D.E.; Lin, C.-J.; Lugovsky, K.S.; Pianori, E.; Robinson, D.J.; et al. The Review of Particle Physics. *Prog. Theor. Exp. Phys.* **2020**, *2020*, 083C01. Available online: https://pdg.lbl.gov/ (accessed on 28 April 2024).
30. Abratenko, P.; Acciarri, R.; Adams, C.; An, R.; Anthony, J.; Asaadi, J.; Auger, M.; Bagby, L.; Balasubramanian, S.; Baller, B.; et al. Determination of muon momentum in the MicroBooNE LArTPC using an improved model of multiple Coulomb scattering. *J. Instrum.* **2017**, *12*, P10010. [CrossRef]
31. Mager, M. ALPIDE, the Monolithic Active Pixel Sensor for the ALICE ITS upgrade. *Nucl. Instrum. Methods Phys. Res. Sect. A Accel. Spectrom. Detect. Assoc. Equip.* **2016**, *824*, 434–438. [CrossRef]
32. Ricci, E. A pixel based tracker for the HEPD-02 detector. In Proceedings of the Science (POS), 38th International Cosmic Ray Conference (ICRC2023), Nagoya, Japan, 26 July–3 August 2023 ; Volume 444. [CrossRef]
33. Savino, U. Expected performance of the High Energy Particle Detector (HEPD-02) tracking system on board of the second China Seismo-Electromagnetic Satellite. *Nucl. Instrum. Methods Phys. Res. Sect. A Accel. Spectrom. Detect. Assoc. Equip.* **2024**, *1063*, 169281. [CrossRef]
34. Allison, J.; Amako, K.; Apostolakis, J.; Araujo, H.; Arce Dubois, P.; Asai, M.; Barrand, G.; Capra, R.; Chauvie, S.; Chytracek, R.; et al. Geant4 developments and applications. *IEEE Trans. Nucl. Sci.* **2006**, *53*, 270–278. [CrossRef]
35. Barlow, R.; Beeston, C. Fitting using finite Monte Carlo samples. *Comp. Phys. Commun.* **1993**, *77*, 219–228. [CrossRef]
36. von Doetinchem, P.; Aramaki, T.; Bando, N.; Boggs, S.; Fuke, H.; Gahbauer, F.; Hailey, C.; Koglin, J.; Mognet, S.; Madden, N.; et al. The flight of the GAPS prototype experiment. *Astropart. Phys.* **2014**, *54*, 93–109. [CrossRef]